Shape-Memory Polymer Networks with Fe_3O_4 Nanoparticles for Remote Activation

Christopher M. Yakacki,[1,2] Nitin S. Satarkar,[3] Ken Gall,[1,2,4] Roxanne Likos,[1,5] J. Zach Hilt[3]

[1]*Research and Development, MedShape Solutions, Atlanta, Georgia 30318*
[2]*School of Materials Science and Engineering, The Georgia Institute of Technology, Atlanta, Georgia 30332*
[3]*Department of Chemical and Materials Engineering, University of Kentucky, Lexington, Kentucky 40506*
[4]*George Woodruff School of Mechanical Engineering, The Georgia Institute of Technology, Atlanta, Georgia 30318*
[5]*Department of Biomedical Engineering, The Georgia Institute of Technology, Atlanta, Georgia 30318*

Received 17 September 2008; accepted 6 December 2008
DOI 10.1002/app.29845
Published online 25 February 2009 in Wiley InterScience (www.interscience.wiley.com).

ABSTRACT: Shape-memory polymers (SMPs) have recently shown the capacity to actuate by remote heating via the incorporation of magnetic nanoparticles into the polymer matrix and exposure to an alternating magnetic field. In this study, methacrylate-based thermoset SMP networks were synthesized through free-radical polymerization with varying amounts of Fe_3O_4 magnetite (0, 1, and 2.5 wt %). Furthermore, the chemistry of the networks was controlled to maintain a constant glass transition temperature (T_g) while varying the degree of chemical crosslinking. Remote heating of the networks was shown to be a direct function of the nanoparticle concentration and independent of the chemistry. Magnetite reinforcement was shown to influence the thermomechanical properties of the networks; increasing Fe_3O_4 concentrations led to decreases in T_g and rubbery modulus. However, networks with a higher degree of crosslinking were more resistant to thermomechanical changes with respect to magnetite concentration. Strain to failure was shown to decrease with the addition of nanoparticles and the free-strain shape-memory cycle was investigated for all of the networks. Networks with lower degrees of crosslinking and high magnetite concentrations showed a significant amount of irrecoverable strain. Last, the use of remotely heated shape-memory materials is discussed in light of potential biomedical applications. © 2009 Wiley Periodicals, Inc. J Appl Polym Sci 112: 3166–3176, 2009

Key words: shape memory polymer; magnetite; remote heating; inductive

INTRODUCTION

Shape-memory polymers (SMPs) are a class of mechanically functional smart materials that are defined by their ability to recover a defined shape after significant mechanical deformation.[1,2] SMPs respond to external stimuli such as heat and light and have been shown to recover strains on the order of 100% or more.[3–7] If constrained, SMPs will generate a recovery stress, which can be used to perform mechanical work. Aside from sensors and actuators,[7,8] SMPs are attractive for medical devices because of their high tailorability,[9] initial biocompatibility results,[10–12] and potential for minimally invasive surgery.[13–18]

Thermoset polymers utilize chemical crosslinks and entropic elasticity to perform shape memory.[19] A typical shape-memory cycle begins by heating the polymer to its glass transition temperature (T_g) to increase chain mobility and molecular motions. Next, the sample is deformed and cooled to store the strains within the sample. This is often referred to as the stored or packaged state. Ideally, the polymer sample will retain its packaged state indefinitely until activated by an external stimulus. The shape-memory effect is activated by reheating the polymer to the vicinity of T_g, in which molecular motions are again enabled and driven by an increase in entropy and reduction in free energy. A thorough review of the shape-memory effect in polymer networks has been published in a previous study.[20]

The majority of SMPs rely on direct heating to thermally initiate the shape-memory effect. In the case of biomedical SMPs, body temperature is suggested as the activation temperature from the naturally regulated heat supply of the body. However, the difference between room and body temperature may not be sufficient to activate the shape-memory effect in a timely manner if the polymer is stable at room temperature. Researchers have investigated alternate methods of heating inside the body including the use of lasers to heat a device at the location of implantation.[21–23]

One alternative method of heating for SMPs *in vivo* is the use of remote heating, which relies on magnetic nanoparticles within the polymer matrix to create

Correspondence to: C. M. Yakacki (chris@medshapesolutions.com).

heat via power loss when exposed to an alternating magnetic field. Figure 1 is an example of a remotely heated shape-memory polymer recovering from a flattened strip to a helix shape. Buckley et al. introduced the concept of using Nickel Zinc Ferrites with tailored Curie temperatures to auto-regulate heating in SMPs.[24] Razzaq et al. studied the electrical and magnetic properties of magnetite (Fe_3O_4) filled polyurethanes with shape-memory.[25] Mohr et al. also studied polyurethane and biodegradable thermoplastics reinforced with magnetite and showed that magnetic activation rates were comparable with standard thermal activation rates.[26] Schmidt studied the effects of magnetite on butyl acrylate networks crosslinked with oligo(ε-caprolactone) dimethacrylate.[27] In addition, the remote heating properties of magnetic nanoparticles have found their way into other functional biomaterials. For example, researchers have investigated the combination of magnetic particles with thermosensitive hydrogels to create a remote controlled (RC) drug delivery platform.[28–30]

Previous studies on induction heating have laid the groundwork to consider the magnetic activation of SMPs. The purpose of this study was to systematically investigate the correlation between polymer crosslinking and magnetic Fe_3O_4 nanoparticles on polymerization, mechanical, thermomechanical, and shape-memory properties of the networks. The results of this study aim to provide fundamental relationships between composite structure and properties, with the ultimate goal of tailoring structure to balance the inherent tradeoffs in activation and thermomechanical shape-memory properties.

MATERIALS AND METHODS

Materials

Methyl methacrylate (MMA), poly(ethylene glycol)$_n$ dimethacrylate (PEGDMA) with a typical M_n of 550, 750, and 1000 g/mol, photoinitiator 2,2-dimethoxy-2-phenylacetophenone (DMPA), and thermal initiator 2,2′-Azobisisobutyronitrile were ordered from Sigma-Aldrich and used as received. Spherical iron-oxide nanoparticles (Fe_3O_4 magnetite) with a mean diameter of 20–30 nm were purchased from Nanostructured and Amorphous Materials Inc.

Composite synthesis

Monomer solutions were created using MMA crosslinked with PEGDMA. The amount and M_n of the PEGDMA was varied to create three polymer networks with similar T_gs and varying rubbery modulus values. The networks were designated 9006, 9011, and 9016 and contain 29.2, 36.2, and 47.0 wt % of PEGDMA crosslinking monomer, respectively. Ethanol was added 50% by weight and nanoparticles were added at loadings of 0, 1, and 2.5 wt % of the monomer mixture (0, 0.227, 0.565 vol %, respectively). The particles were dispersed uniformly in the solution by probe sonication (Fisher Scientific, Sonic Dismembrator Model 500) for 5 min followed by sonication in an ultrasonic bath for 30 min. The photoinitiator and thermal initiator were added at 1 wt % each of the total monomer mixture and their complete dissolution was insured by bath sonication. The solutions were then pipetted into a mold of two 15 × 15 cm^2 glass plates separated by a 500-μm Teflon spacer. The mold was then transferred to a UV source (LESCO, FEM 1011) with a wavelength 365 nm and intensity 17.5 mW/cm^2. Polymerization was carried out for 5 min. Uniform intensity on both sides of the film was ensured during polymerization. The mold was then immediately removed and placed in an oven at 55°C for 24 h to increase overall conversion. The polymer film was then removed from the mold and placed in deionized water. Each composite film was washed daily by changing its water until no significant monomers were observed in the wash water. The films were then dried in air followed by a vacuum oven for 24 h.

Conversion analysis

Conversion of the composites were analyzed using attenuated total reflectance Fourier transformed infrared spectroscopy (ATR-FTIR). First, the IR spectrum of the monomer solution was collected. After the

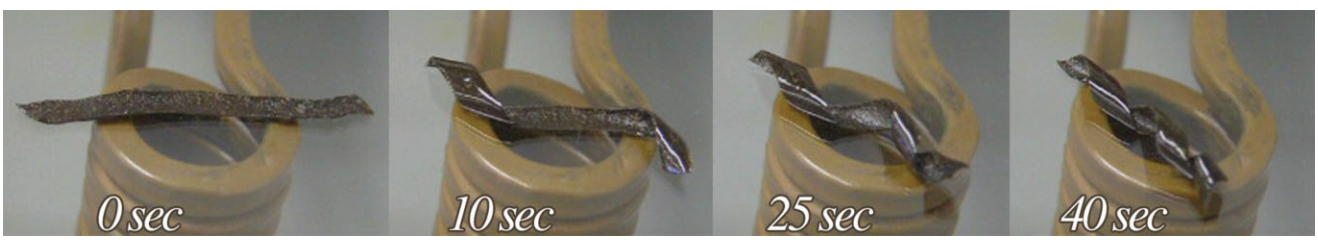

Figure 1 Fe_3O_4-reinforced shape-memory polymer recovering from a flattened sheet to a helix using remote heating for activation. [Color figure can be viewed in the online issue, which is available at www.interscience.wiley.com.]

polymerization was complete, the IR spectrum of the nanocomposite surface was collected on both sides of the composite film. The conversion of the monomers were determined by standard baseline techniques using the peak area of the 1636 cm^{-1} for C=C vibration and the area of 1716 cm^{-1} for C=O stretching as reference. The conversion of the double bond was determined from the following formula:

$$\xi = 1 - \frac{C}{U} \quad (1)$$

Where C is the ratio of peak area of the C=C to the reference peak area of C=O after polymerization, and U is the ratio of same peak area of the prepolymer solution.

SEM analysis

The morphology of composites and nanoparticle dispersion was analyzed using scanning electron microscopy (Hitachi, S4300). The samples were freeze-fractured and cross-sectional images were taken for 0, 1, and 2.5% particle loaded 9016 systems.

Remote heating on exposure to alternating magnetic field

The heating response of composites exposed to an alternating magnetic field (AMF) was characterized using an induction power supply (Taylor Winfield, MMF-3-135/400-2). Polymer discs were cut in to 15 mm diameters and placed in a glass Petri dish on top of the solenoid (15 mm diameter, five turns) to get AMF strength of 33×10^{-4} T and frequency 297 kHz. An IR camera (AGEMA, Thermovision 470) was used to record surface temperatures of the discs. The field heating was continued for 5 min, and results were averaged over three samples.

Dynamic mechanical analysis

Rectangular samples with dimensions of approximately $0.4 \times 3 \times 25$ mm^3 were cut and secured in the dynamic mechanical analysis (DMA) tensile fixture for glass transition tests using a TA Instruments Q800. Active sample length (grip displacement) was $\sim$ 10 mm for all tests. Testing was performed under 0.1% oscillating strain control using a force track of 150%. Samples were thermally equilibrated at 0°C for 3 min, and then heated to 180°C at a rate of 5°C per minute. Samples were run in triplicate. The onset of glass transition (T_{onset}) was calculated by the intersecting line method, with the starting point of the left intersecting line at 30°C less than T_g, and the right intersecting line at T_g. The breadth of the glass transition ($T_{breadth}$) was defined as twice the difference of T_g and T_{onset}.

Strain-to-failure testing

Strain-to-failure testing was performed by using an Instron 5567 Universal Testing Machine equipped with an environmental chamber. Tapered samples were cut using a steel punch and a plate press then polished using 600-grit silicon carbide sandpaper to remove edge defects caused by the punch. The samples had a gauge length of 25.5 mm and a width of 4 mm at the thinnest region. The spring-loaded tensile clamps used to secure the samples were lined with 600-grit silicon carbide sandpaper to prevent the samples from slipping in the clamps during testing. The samples were equilibrated to room temperature (22 ± 1°C) inside of the Instron environmental chamber for at least 1 min and were then preloaded to 0 N. The samples were extended at a rate of 0.1% per second until failure.

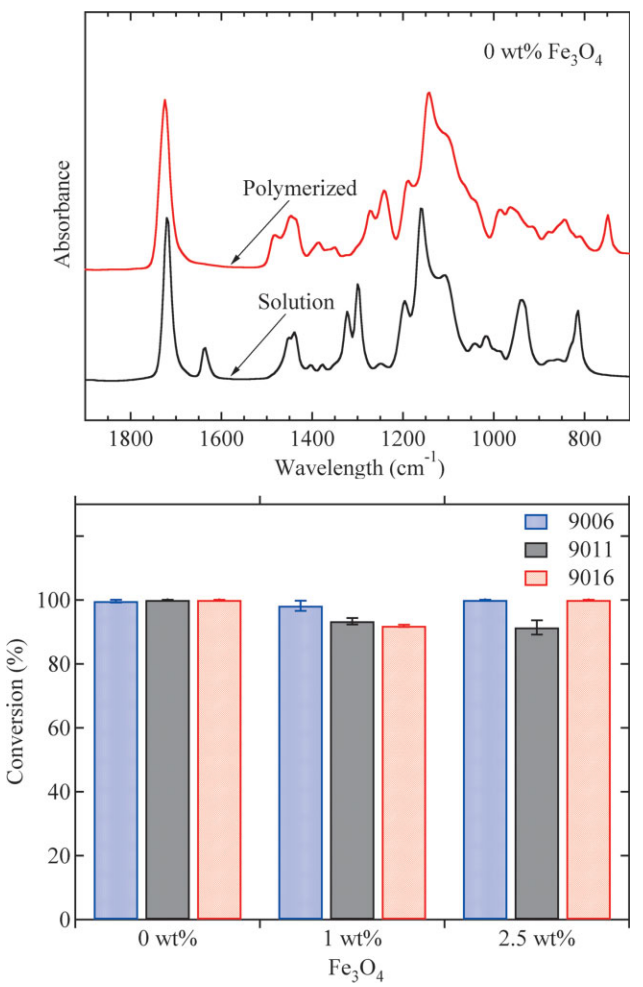

Figure 2 (a) FTIR analysis of the starting monomer solution and final polymer. (b) Conversion of all the nine polymer networks. [Color figure can be viewed in the online issue, which is available at www.interscience.wiley.com.]

Free-strain recovery characterization

Free-strain recovery testing was performed using the DMA under a similar protocol created by Kunzelman et al.[7] Samples identical to glass transition testing were thermally equilibrated at 85°C for 1 min before the data were recorded. Stress was then increased from 0 to 1.0 MPa at a rate of 0.01 MPa per second and fixed at 1.0 MPa while temperature cooled to 0°C at a rate of 5°C per minute. The temperature was equilibrated at 0°C for 1 min, then stress isothermally unloaded back to 0 MPa at 0.01 MPa per second. Finally, free-strain recovery was measured as the temperature was increased to 110°C at a rate of 5°C per minute. The strain recovery ratio was defined as:

$$\varepsilon_r = \frac{\varepsilon_{max} - \varepsilon_{final}}{\varepsilon_{max}} \quad (2)$$

where ε_r is the strain recovery ratio, ε_{max} is the maximum strain experience during deformation and cooling, and ε_{final} is the final strain value after heating.

RESULTS

The method for calculating the conversion is shown in Figure 2(a), which shows the reduction in absorbance at 1636 cm^{-1} for C=C vibrations in the acrylic double bonds. For high conversions, the polymerizations showed approximately a complete disappearance of the absorbance peak at 1636 cm^{-1}. The conversions of the polymer networks are shown in Figure 2(b). Near complete conversion is reached for the virgin networks containing no Fe_3O_4 nanoparticles. The 9006 networks showed near complete conversion for both nanoparticle concentrations. The 9011 network dropped to 93 and 91% conversion for the 1 and 2.5 wt % compositions, respectively. In the 9016 networks, a slight drop in conversion to 92% was seen for the 1 wt % composition, though near complete conversion was seen in the 2.5 wt % composition.

SEM analysis of the cross-sectional view of the virgin and reinforced polymers are shown in Figure 3. The bottom set of photographs shows the samples at 10× more magnification than the top set. The virgin networks containing no Fe_3O_4 nanoparticles show smoother fracture planes than the reinforced networks. The 2.5 wt % reinforced network shows the most irregular fracture plane, which is better shown in the lower magnification image.

Heating was assessed via infrared imaging. Figure 4(a) shows the infrared images of the 9006 network with 2.5 wt % Fe_3O_4 being heated over a 5-min period. The heating profiles of all nine networks as a function of time are summarized in Figure 4(b). In general, all of the networks started at room temperature and experienced continued heating. The networks with 2.5 wt % Fe_3O_4 experienced the greatest heating and all reached 51.7°C after 5 min while the networks with 1.0 wt % Fe_3O_4 reached temperatures between 38 and 41°C. As a baseline for comparison, the networks with 0 wt % were measured and experienced an increase of ~ 7°C above room temperature to 30°C.

Representative glass transitions of the networks are shown in Figure 5. For a complete listing of thermomechanical properties, refer to Table I. Figure 5(a)

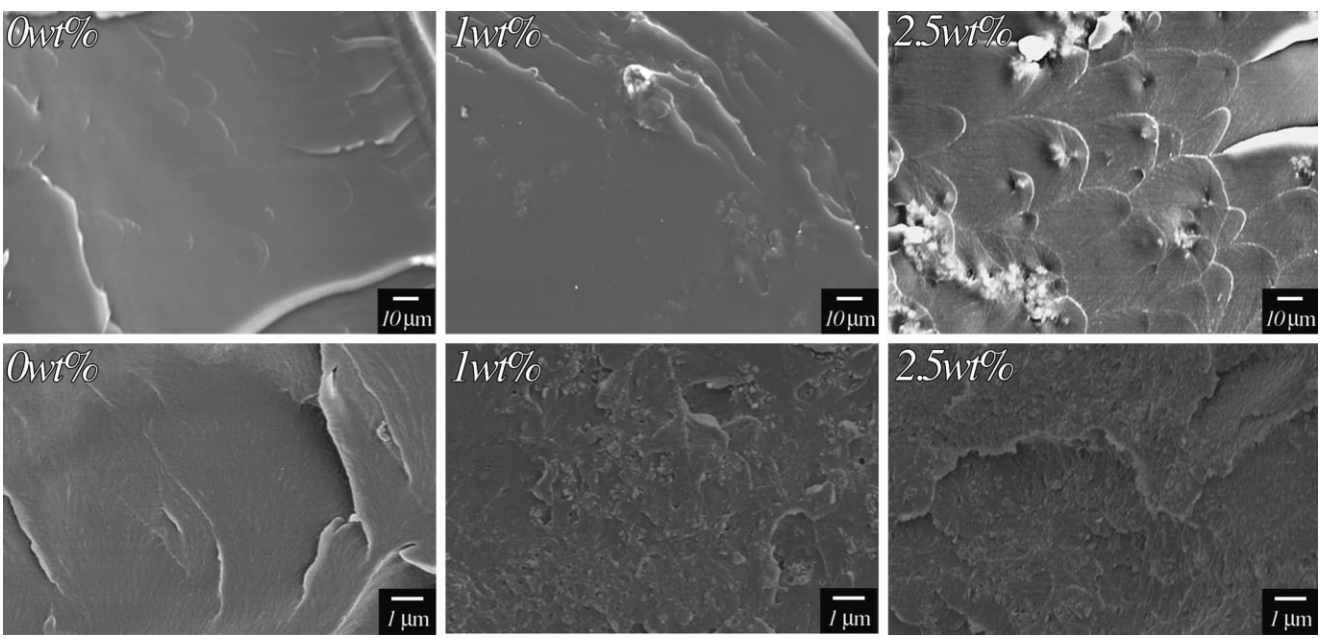

Figure 3 SEM analysis of 0, 1, and 2.5 wt % Fe_3O_4 networks at low (top) and high (bottom) magnifications.

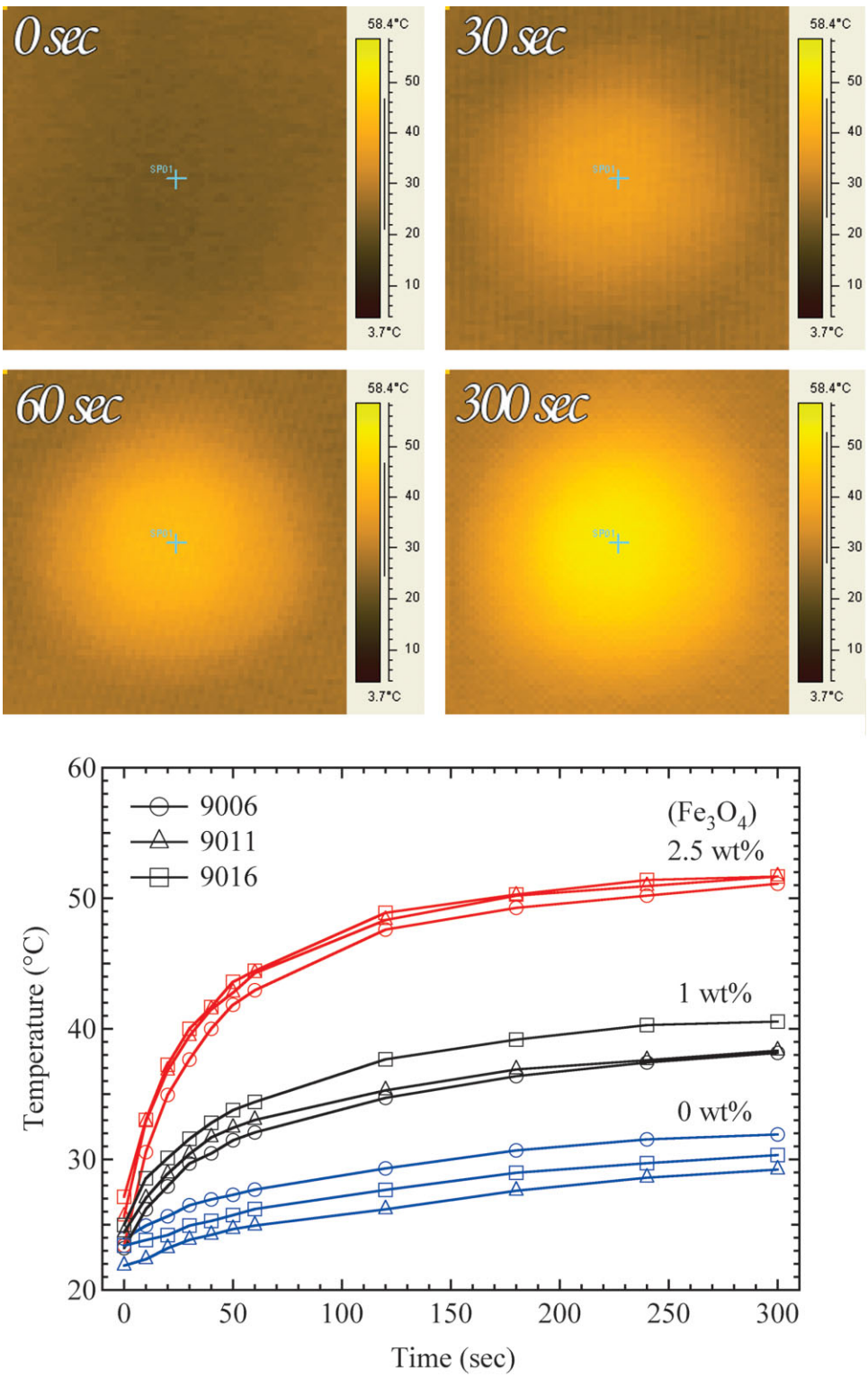

Figure 4 (a) Image analysis of heating a 2.5 wt % Fe_3O_4 sample. (b) Heating profiles of the nine networks over time. [Color figure can be viewed in the online issue, which is available at www.interscience.wiley.com.]

shows a baseline comparison of the three networks without any addition of nanoparticles. The 9006, 9011, and 9016 networks had starting T_g values of 85, 88, and 82°C, respectively, which is comparably equal based on standard error. Figure 5(b,c) show a slight decrease in T_g and rubbery modulus with the addition of nanoparticles. For both the 9006 and 9011 networks, there is a 6°C drop in T_g with the addition of

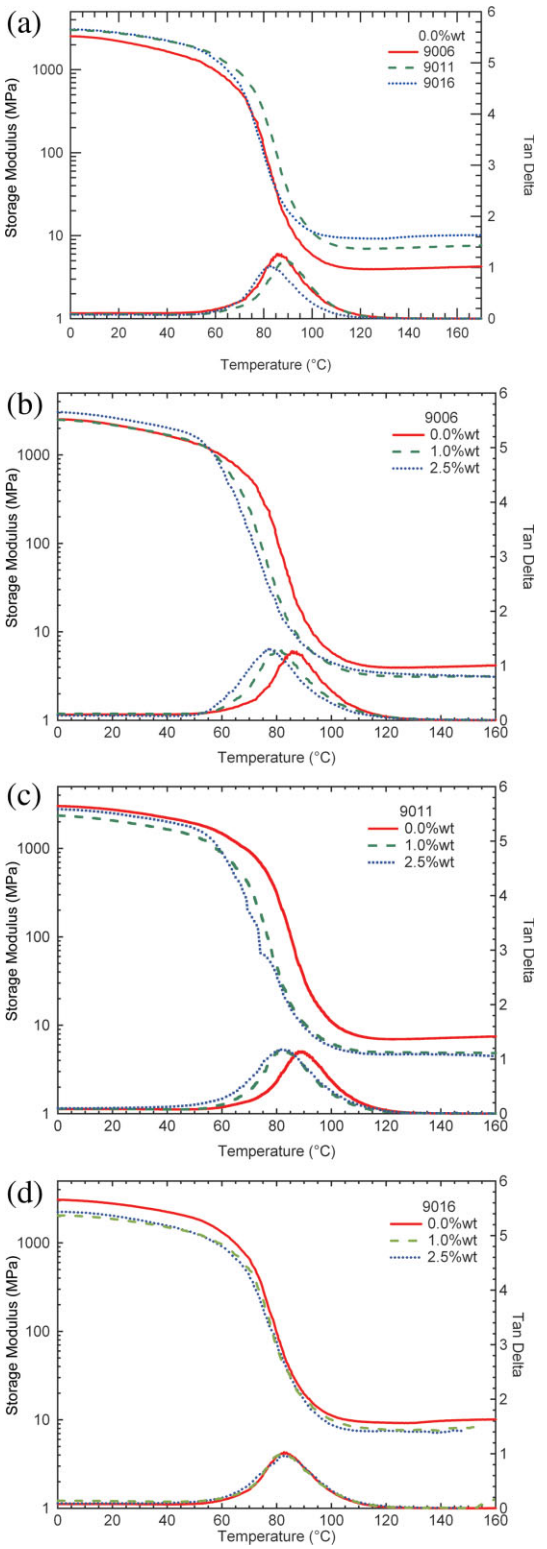

Figure 5 Glass transitions of the networks. (a) A comparison of the 9006, 9011, and 9016 networks with 0 wt % Fe_3O_4. (b) Glass transitions of the networks with 0, 1, and 2.5 wt % Fe_3O_4 for the 9006. (c) 9011 and (d) 9016 polymer systems. [Color figure can be viewed in the online issue, which is available at www.interscience.wiley.com.]

1 wt % particles, and a further reduction of 3 to 4°C with the addition of 2.5 wt % Fe_3O_4. Both the 9006 and 9011 networks showed a steady reduction in rubbery modulus with the increased addition of Fe_3O_4. Furthermore, both networks showed an increase in breadth of the glass transition with increasing particle content. Figure 5(d) shows that the 9016 networks were resistant to any appreciable drop in T_{onset}, T_g, or $T_{breadth}$ with the addition of Fe_3O_4. However, the 9016 network did show a drop in rubbery modulus with an increase in Fe_3O_4 particles.

Strain-to-failure of the networks at room temperature ($\sim$ 22°C) are shown in Figure 6. Figure 6(a) shows that the maximum failure strain (ε_f) for the 9006 network starts at 60.3% and decreases to 31.2 and 12% with the addition of 1 and 2.5 wt % Fe_3O_4, respectively. This decreasing failure-strain trend is also seen in Figure 6(b,c). The 9011 networks has failure strains decrease from 15.2 to 7.6% while the 9016 network shows a decrease from 11.6 to 5%. A summary of the strain-to-failure data can also be seen in Table I.

Free-strain recovery testing was performed on all of the polymer samples and results are presented in Figure 7. Figure 7(a) is a baseline comparison of all three networks without the addition of Fe_3O_4 nanoparticles. In all the tests, the networks are stressed to and held at 1 MPa during the stretching and cooling stages. The strain once 1 MPa stress is reached is defined as ε_{1MPa}, though the networks continue to elongate during the cooling stage. In the 9006 networks [Fig. 7(b)], the 0 and 1 wt % samples reach of maximum strain state (ε_{max}) of 39 and 51%, respectively. On heating, both samples recover to 3% strain. The 2.5% reinforced network shows a severe creep response at the end of the deformation stage and beginning of the cooling stage. The 2.5% sample reaches a maximum temporary strain of 91.8 and recovers 54.1% strain, leaving 37.7% in unrecoverable plastic strain. The recovery cycle of the 9011 network samples can be seen in Figure 7(c). The maximum temporary strains in these samples are less than the 9006 samples; however, they show the same trend of higher overall strains from reinforced samples than the unreinforced samples. All the samples recover to $\sim$ 2 to 3% final strain (ε_{final}) giving a strain recovery ratio of $\sim$ 90%. The 9016 network samples are shown in Figure 7(d) and experience about half of the maximum temporary strain compared with the 9011 samples. The 0 and 1% samples exhibit nearly identical shape-recovery cycles while the 2.5% Fe_3O_4 initially is more resistant to deformation, but then experiences a gradual elongation during the cooling process. All three samples recover to $\sim$ 1 to 1.5% strain giving strain recovery ratios of $\sim$ 92%. A summary of the strains and recovery ratios of the samples can be seen in Table II.

TABLE I
A Summary of the Thermomechanical Properties of the Nine Networks

Material	Fe_3O_4 (wt %)	T_{onset} (°C)	T_g (°C)	$T_{breadth}$ (°C)	R.M. (MPa)	ε_f (%)
	0.0	73.9 ± 2.8	85.2 ± 1.3	22.7 ± 3.0	3.6 ± 0.8	60.3 ± 4.8
9006	1.0	67.5 ± 1.9	80.2 ± 0.7	25.4 ± 2.4	3.2 ± 0.1	31.2 ± 6.8
	2.5	63.9 ± 2.3	78.6 ± 1.7	29.3 ± 3.2	2.6 ± 0.5	12.0 ± 1.8
	0.0	76.2 ± 2.2	88.0 ± 1.8	23.6 ± 2.7	6.6 ± 0.4	15.2 ± 3.8
9011	1.0	70.4 ± 1.3	82.8 ± 0.6	24.9 ± 1.6	4.4 ± 0.9	13.5 ± 2.0
	2.5	67.4 ± 1.3	81.7 ± 0.4	28.5 ± 2.1	3.1 ± 1.1	7.6 ± 0.3
	0.0	68.3 ± 2.8	81.7 ± 2.4	26.8 ± 1.4	7.6 ± 2.3	11.6 ± 1.2
9016	1.0	69.5 ± 2.6	81.2 ± 1.6	23.3 ± 4.1	6.6 ± 1.4	5.8 ± 1.1
	2.5	69.4 ± 0.4	82.3 ± 2.1	25.7 ± 4.3	5.4 ± 1.2	5.0 ± 0.6

DISCUSSION

A SMP system based on MMA and PEGDMA was chosen for its high degree of tailorability. The polymer's thermomechanical properties, such as T_g and rubbery modulus, were controlled by varying the amount and molecular weight of the PEGDMA crosslinking monomer, which has been shown effective in other studies.[3,14] In this study, three polymer systems (nine networks) were designed to have a relatively constant T_g and varied rubbery modulus to investigate how network crosslinking would effect conversion, heating, thermomechanical properties, and shape recovery in the presence of magnetite nanoparticles.

The 9006, 9011, and 9016 networks were designed to have a T_g of 85°C with increasing rubbery modulus values. The amount of PEGDMA crosslinking monomer used in the three networks increased from 29.2, 36.2, and 47.0 wt % for the respective networks. The full conversion of all three systems without the addition of Fe_3O_4 particles is shown in Figure 2. Decreases in conversion were noticed in several of the networks with the addition of magnetite. However, full conversion was still seen in the lowest and highest crosslinking systems with the highest amount of magnetite. Conversion was the lowest for the 9011 network with 2.5 wt % Fe_3 O_4 at 91%, which is still high enough to verify reasonable efficacy of the polymerization method with and without the addition of the nanoparticles.

The conversion data from FTIR analysis from Figure 2 should be compared against the DMA shown in Figure 5 and Table I. As previously stated, the FTIR analysis did detect a decrease in conversion for several of the networks with the addition of nanoparticles. Consequently, more insight into this trend can be seen by evaluating the rubbery modulus values from DMA. The rubbery modulus is an indication of elastically effective crosslinking density within a polymer network. The rubbery modulus increases from the 9006 to the 9016 networks is driven by the addition of more crosslinking monomer in the latter material. With the addition of nanoparticles, the rubbery modulus decreases significantly for all the networks. This agrees with observations seen by Schmidt in a previous study, in which composite networks showed a higher degree of swelling due to a lower crosslinking density caused by the particles.[27] Furthermore, the T_g of the 9006 and 9011 networks are reduced by $\sim$ 6 and 3.5°C with the addition of 1 and 2.5 wt % nanoparticles, respectively. Conversely, the glass transition is relatively unaffected for the 9016 network. T_{onset}, T_g, and $T_{breadth}$ all remain unaffected with the addition of nanoparticles. This data suggests that polymer networks with higher degrees of crosslinking are less sensitive to changes in thermomechanical properties with the addition of nanoparticulate reinforcement.

The SEM photographs represented in Figure 3 show the cross-sectional fracture planes of the polymer matrices. The lower magnification images of the 2.5 wt % samples illustrate areas of nanoparticles agglomerations. The mechanical effects of these particles in the polymer matrix can be seen in the strain-to-failure tests in Figure 6. Recent work has shown that the optimal temperature to deform shape-memory polymers is around T_{onset}[3]; however, this testing was done at room temperature to give information on the mechanical properties at a typical handling temperature. The strain-to-failure decreases from the 9006 to the 9016 networks, which is because of an increase in crosslinking and reduction in network mobility. The reduction in strain-to-failure is most significant in the 9006 network, which reduces from 60 to 12%. Even though the remaining 9011 and 9016 networks experience less overall reductions in strain-to-failure, it is important to note that the addition of particles embrittles the polymers by eliminating its ability to yield during deformation. Although the higher crosslinked networks are still able to undergo larger deformations at elevated temperature, they become more brittle at typical handling temperatures (22°C).

The heating profiles of all the samples are shown in Figure 4. The 0 wt % unreinforced networks experience $\sim$ 7°C of heating due to resistive heating. However, a clear and statistically significant amount of

heating is seen in the 1 and 2.5 wt % filled networks. All of the 1 wt % networks heated to 38–41°C while the 2.5 wt % networks heated to 51.7°C. Though these data show that heat generation is increased by increasing the amount of magnetite particles, it also shows that heat generation is not restricted by the polymer structure and is primarily governed by the amount of Fe_3O_4 added within the matrix. It has been previously demonstrated that the magnetic field strength directly controls the heating of the particles and therefore stronger field strength would produce higher levels of heating.[26] However, this effect was not investigated further in this study because of machine limitations. It also should be noted that the material example of Figure 1 had a lower T_g ($\sim$ 65°) than compared with the networks in this study to show rapid recovery of the device. This does not diminish the current results as it has been shown that the temperature response of shape-memory polymers shifts evenly and directly with temperature shifts in T_g given a constant crosslinking density.[31]

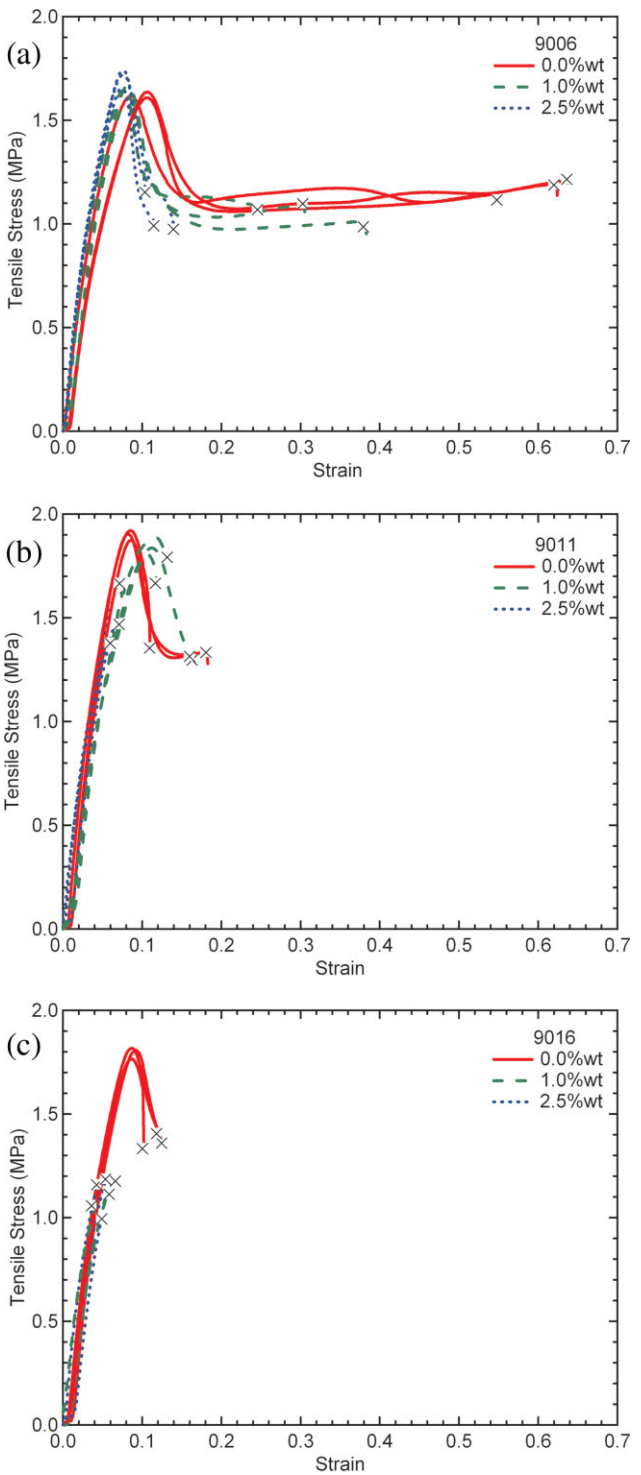

Figure 6 Strain to failure for (a) 9006, (b) 9011, and (c) 9016 networks. [Color figure can be viewed in the online issue, which is available at www.interscience.wiley.com.]

Free-strain shape recovery testing is shown in Figure 7. Because the deformation of the samples occurred at T_g ($\sim$ 85°C), the samples showed a higher strain capacity than presented in Figure 6. By taking the amount of strain at 1 MPa (ε_{1MPa}) during the deformation stage, a quasistatic rubbery modulus can be estimated using Hooke's Law, $E = \sigma/\varepsilon$, for the samples. Using this releationship, 3.6, 6.8, and 8.1 MPa would be the estimated quasistatic rubbery modulus values for the 9006, 9011, and 9016 networks, respectively, which is consistent with the DMA results. After the deformation stage is complete, the samples will experience some amount of elongation as they cool. This elongation is because of the viscous effects caused by the stress-loading rate during deformation. These elastic and viscous strains (elastic and/or plastic) are primarily recovered upon reheating through the glass transition. However, for the 9006 network with 2.5 wt % Fe_3O_4, a large visco-plastic creep response was seen during the cooling stage. The sample crept $\sim$ 50%, which was unrecoverable during reheating. The only sample to experience significant creep was the materials with the lowest crosslinker concentration and highest particle loading. The diminishing conversion imparted by increased particle concentration, coupled with the relatively low concentration of crosslinker, creates a material with the lowest effective crosslink density and smallest resistance to plastic flow.

It is insightful to discuss the results from an overarching perspective to guide the design and selection of a magnetic-particle reinforced SMP. The heat generation results from Figure 4 might suggest that the choice of polymer network does not matter, and a high amount of magnetite filler should be used to maximize heat generation. Alternatively, the heating effect can be enhanced by increasing the strength of applied magnetic field. Conversion and DMA results from Figures 2 and 5 suggest that a polymer with a high degree of crosslinking should be used to prevent a depression in T_g while broadening the glass transition. Conversely, the strain-to-failure results of Figure

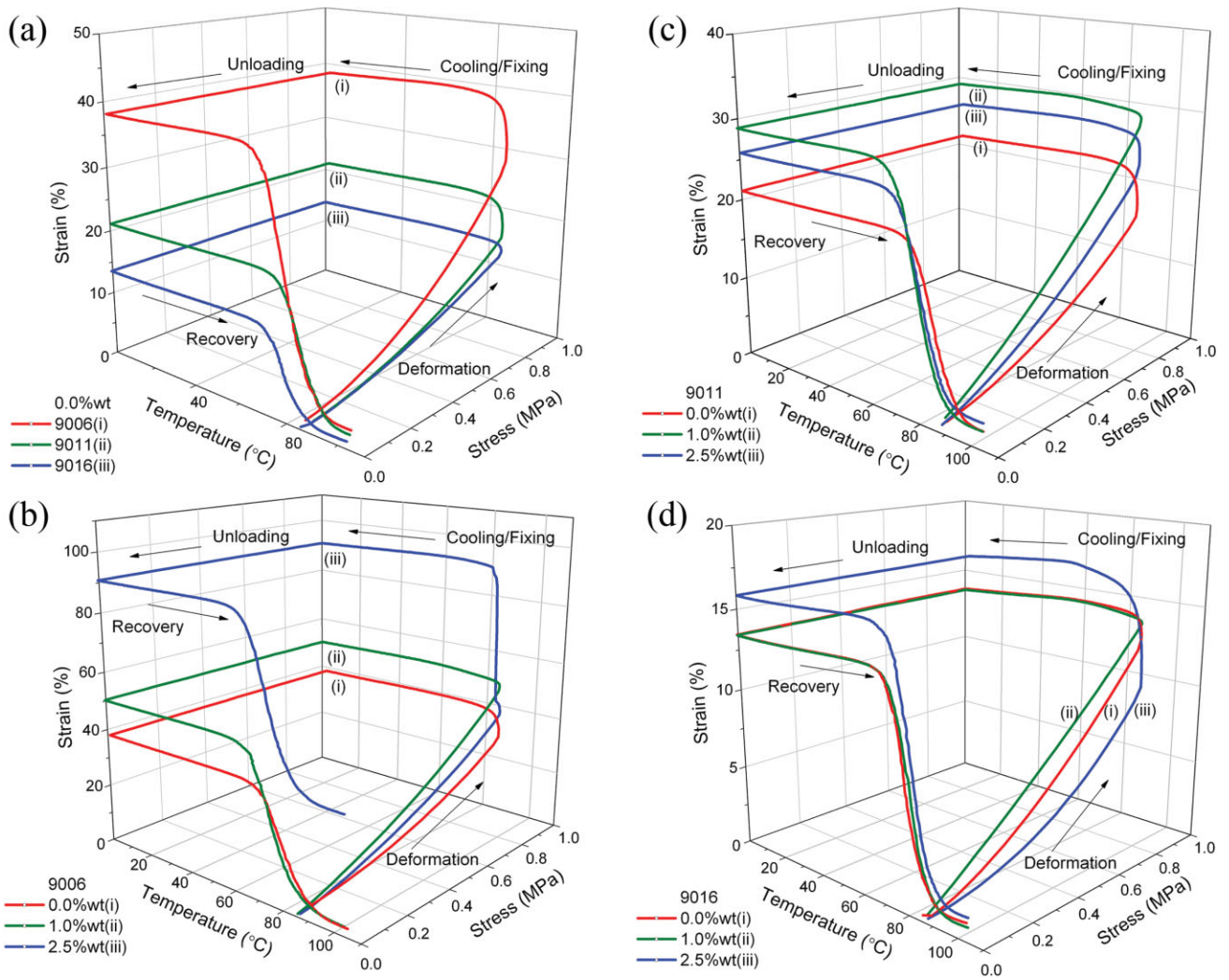

Figure 7 Free-strain recovery profiles of the networks. (a) A comparison of the 9006, 9011, and 9016 networks with 0 wt % Fe_3O_4. (b) Free-strain recovery of the networks with 0, 1, and 2.5 wt % Fe_3O_4 for the 9006 (c) 9011 and (d) 9016 polymer systems. [Color figure can be viewed in the online issue, which is available at www.interscience.wiley.com.]

6 would suggest using a polymer with a lower degree of crosslinking to maximize failure strains and prevent polymer embrittlement at room temperature. However, the free-strain recovery tests of Figure 7 would show that low levels of crosslinking and high levels of magnetite lead to unrecoverable strains due to viscoplasticity. Although we have not sought after the "optimal" composition in this work, we have demonstrated the tradeoffs in recoverability and thermomechanical properties inhernet to SMP composites. It is important that these tradeoffs are carefully considered when designing for a specific application.

TABLE II
A Summary of Strains and Recovery of Free-Strain Recovery Experiments

Material	Fe_3O_4 (wt %)	ε_{1MPa} (%)	ε_{max} (%)	ε_{final} (%)	Recovery ratio (%)
9006	0.0	28.0	39.1	3.0	92.3
	1.0	45.4	51.0	3.2	93.7
	2.5	36.5	91.8	37.7	59.0
9011	0.0	14.8	21.9	2.3	89.6
	1.0	27.0	29.6	2.2	92.4
	2.5	21.8	26.7	3.2	88.0
9016	0.0	12.3	14.2	1.1	92.2
	1.0	13.3	14.1	0.9	93.8
	2.5	9.1	16.6	1.5	91.3

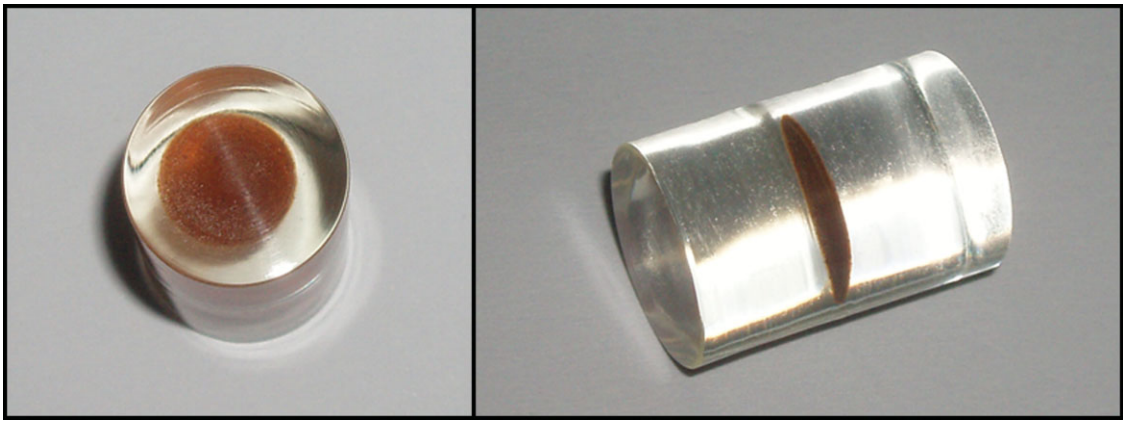

Figure 8 A composite shape-memory polymer sample containing a 2.5 wt % reinforced center. [Color figure can be viewed in the online issue, which is available at www.interscience.wiley.com.]

For example, the magnetically activated helix in Figure 1 may need a high degree of crosslinking to achieve self-deployment in a constrained environment at the risk of lowering its failure strains. Other applications for this technology should be explored and investigated. Composites of this material with traditional SMPs provide an opportunity to heat a device from its core. Figure 8 is an example of a 2.5 wt % Fe_3O_4 disk polymerized inside of regular shape-memory polymer. This would offer the advantage of maintaining mechanical properties regardless of the heating element. Furthermore, in biomaterials it would shield the body from the magnetite. This presents a unique set of opportunities in creating and designing remotely activated shape-memory polymers for various applications.

CONCLUSIONS

Heating of the Fe_3O_4-filled SMPs were directly influenced by the concentration of magnetite and were not influenced by the crosslink density of the networks. Incorporation of the magnetite showed a decrease in crosslinking density via reduction of the rubbery modulus; however, the glass transition was least affected in the highest crosslinked network. A decrease in strain-to-failure was observed with an increase in nanoparticle concentration, which led to a brittle behavior in highly crosslinked networks deformed at room temperature. Magnetite-filled systems were shown to recover large amounts of strain under free-strain recovery conditions, though lightly crosslinked systems with high particle concentration experience a significant amount of irrecoverable (plastic) strains. In summary, the networks showed a relatively high degree of mechanical and thermal tailorability for use in future remotely heated shape-memory devices.

The authors thank Wenchao Li and Katy Shaffer for their contributions to this work and Dr. Dipti Biswal for assistance with SEM imaging.

References

1. Wei, Z. G.; Sandstrom, R.; Miyazaki, S. J Mater Sci 1998, 33, 3743.
2. Ratna, D.; Karger-Kocsis, J. J Mater Sci 2008, 43, 254.
3. Yakacki, C. M.; Willis, S.; Luders, C.; Gall, K. Adv Eng Mater 2008, 10, 112.
4. Behl, M.; Lendlein, A. Mater Today 2007, 10, 20.
5. Lendlein, A.; Jiang, H. Y.; Junger, O.; Langer, R. Nature 2005, 434, 879.
6. Behl, M.; Lendlein, A. Soft Matter 2007, 3, 58.
7. Kunzelman, J.; Chung, T.; Mather, P. T.; Weder, C. J Mater Chem 2008, 18, 1082.
8. Gall, K.; Kreiner, P.; Turner, D.; Hulse, M. J Microelectromechan Syst 2004, 13, 472.
9. Liu, C.; Mather, P. T. J Appl Med Polym 2002, 6, 47.
10. Yakacki, C. M.; Lyons, M. B.; Rech, B.; Gall, K.; Shandas, R. Biomed Mater 2008, 3, 015010.
11. Rickert, D.; Lendlein, A.; Schmidt, A. M.; Kelch, S.; Roehlke, W.; Fuhrmann, R.; Franke, R. P. J Biomed Mater Res B Appl Biomater 2003, 67, 722.
12. Cabanlit, M.; Maitland, D.; Wilson, T.; Simon, S.; Wun, T.; Gershwin, M. E.; Van de Water, J. Macromol Biosci 2007, 7, 48.
13. Baer, G.; Wilson, T. S.; Matthews, D. L.; Maitland, D. J. J Appl Polym Sci 2007, 103, 3882.
14. Yakacki, C. M.; Shandas, R.; Lanning, C.; Rech, B.; Eckstein, A.; Gall, K. Biomaterials 2007, 28, 2255.
15. El Feninat, F.; Laroche, G.; Fiset, M.; Mantovani, D. Adv Eng Mater 2002, 4, 91.
16. Sokolowski, W.; Metcalfe, A.; Hayashi, S.; Yahia, L.; Raymond, J. Biomed Mater 2007, 2, S23.
17. Wache, H. M.; Tartakowska, D. J.; Hentrich, A.; Wagner, M. H. J Mater Sci-Mater Med 2003, 14, 109.
18. Lendlein, A.; Kelch, S. Clin Hemorheol Microcirculation 2005, 32, 105.
19. Liu, C.; Qin, H.; Mather, P. T. J Mater Chem 2007, 17, 1543.
20. Gall, K.; Yakacki, C. M.; Liu, Y. P.; Shandas, R.; Willett, N.; Anseth, K. S. J Biomed Mater Res Part A 2005, 73, 339.
21. Maitland, D. J.; Metzger, M. F.; Schumann, D.; Lee, A.; Wilson, T. S. Lasers Surg Med 2002, 30, 1.

22. Baer, G. M.; Iv; Small, W.; Wilson, T. S.; Benett, W. J.; Matthews, D. L.; Hartman, J.; Maitland, D. J. Biomed Eng Online 2007, 6.
23. Small, W.; Wilson, T. S.; Benett, W. J.; Loge, J. M.; Maitland, D. J. Laser-activated shape memory polymer intravascular thrombectomy device.Opt Exp 2005, 13, 8204.
24. Buckley, P. R.; McKinley, G. H.; Wilson, T. S.; Small, W.; Benett, W. J.; Bearinger, J. P.; McElfresh, M. W.; Maitland, D. J. IEEE Trans Biomed Eng 2006, 53, 2075.
25. Razzaq, M. Y.; Anhalt, M.; Frormann, L.; Weidenfeller, B. Mater Sci Eng A 2007, 444, 227.
26. Mohr, R.; Kratz, K.; Weigel, T.; Lucka-Gabor, M.; Moneke, M.; Lendlein, A. Proc Natl Acad Sci USA 2006, 103, 3540.
27. Schmidt, A. M.; Macromol Rapid Commun 2006, 27, 1168.
28. Muller-Schulte, D.; Schmitz-Rode, T. J Magnet Magnet Mater 2006, 302, 267.
29. Frimpong, R. A.; Fraser, S.; Hilt, J. Z. J Biomed Mater Res A 2007, 80, 1.
30. Satarkar, N. S.; Hilt, J. Z. Acta Biomaterialia 2008, 4, 11.
31. Yakacki, C. M.; Shandas, R.; Safranski, D.; Ortega, A. M.; Sassaman, K.; Gall, K. Adv Funct Mater 2008, 18, 2428.